ACS APPLIED MATERIALS & INTERFACES

Research Article

www.acsami.org

3D Polyaniline Porous Layer Anchored Pillared Graphene Sheets: Enhanced Interface Joined with High Conductivity for Better Charge Storage Applications

Pandiaraj Sekar,[†,‡] Bihag Anothumakkool,[†,‡] and Sreekumar Kurungot*[,†,‡]

[†]Physical and Materials Chemistry Division, CSIR-National Chemical Laboratory, Dr. Homi Bhabha Road, Pune 411008, India

[‡]Academy of Scientific and Innovative Research (AcSIR), Anusandhan Bhawan, 2, Rafi Marg, New Delhi 110 001, India

Supporting Information

ABSTRACT: Here, we report synthesis of a 3-dimensional (3D) porous polyaniline (PANI) anchored on pillared graphene (G-PANI-PA) as an efficient charge storage material for supercapacitor applications. Benzoic acid (BA) anchored graphene, having spatially separated graphene layers (G-Bz-COOH), was used as a structure controlling support whereas 3D PANI growth has been achieved by a simple chemical oxidation of aniline in the presence of phytic acid (PA). The BA groups on G-Bz-COOH play a critical role in preventing the restacking of graphene to achieve a high surface area of 472 m^2/g compared to reduced graphene oxide (RGO, 290 m^2/g). The carboxylic acid (−COOH) group controls the rate of polymerization to achieve a compact polymer structure with micropores whereas the chelating nature of PA plays a crucial role to achieve the 3D growth pattern of PANI. This type of controlled interplay helps G-PANI-PA to achieve a high conductivity of 3.74 S/cm all the while maintaining a high surface area of 330 m^2/g compared to PANI-PA (0.4 S/cm and 60 m^2/g). G-PANI-PA thus conceives the characteristics required for facile charge mobility during fast charge−discharge cycles, which results in a high specific capacitance of 652 F/g for the composite. Owing to the high surface area along with high conductivity, G-PANI-PA displays a stable specific capacitance of 547 F/g even with a high mass loading of 3 mg/cm^2, an enhanced areal capacitance of 1.52 F/cm^2, and a volumetric capacitance of 122 F/cm^3. The reduced charge-transfer resistance (RCT) of 0.67 Ω displayed by G-PANI-PA compared to pure PANI (0.79 Ω) stands out as valid evidence of the improved charge mobility achieved by the system by growing the 3D PANI layer along the spatially separated layers of the graphene sheets. The low RCT helps the system to display capacitance retention as high as 65% even under a high current dragging condition of 10 A/g. High charge/discharge rates and good cycling stability are the other highlights of the supercapacitor system derived from this composite material.

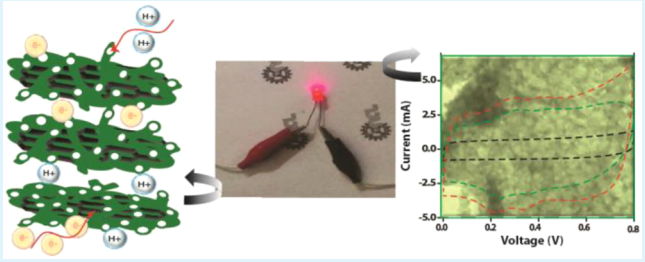

KEYWORDS: *polyaniline, restacking, pillaring, phytic acid, ionic accessibility, durability*

1. INTRODUCTION

A supercapacitor or an ultracapacitor is an ideal candidate for energy storage applications where high power rate is required.[1−3] In modern power electronics, supercapacitors are getting more attention especially because of their unique features like high power density, quick response, long cycle life, easy mode of operation, etc.[4,5] The electrode materials tested for supercapacitors mainly include different carbon morphologies, metal oxides, conducting polymers, etc.[6−9] Among them, polyaniline (PANI) has been studied extensively owing to its high theoretical capacitance, eco-friendly nature, and low cost.[10,11] Compared to bulk, nanomorphologies of PANI (nanotubes, fibers, hierarchical structures, etc.) are preferred because of their superior charge storage properties resulting from the better ionic accessibility and high surface area.[12−15] However, the general synthetic strategies adopted to establish the favorable morphological features to PANI are complicated because of the use of soft and hard templates, which requires an additional step of template removal, which further creates more macropores (>100 nm) than micropores. In addition, the resulting materials generally show diminished electrical conductivity due to the low packing density and discontinuity in the polymer grains. In such cases, when the thickness of the electrode increases, the ion needs to travel a long distance from the electrode to the interface (electrode/electrolyte), which ultimately leads to a drop in the capacitance by a factor of 2−3.[16]

Thus, to see PANI as an electrode material in commercial supercapacitors, the key point is to address the trade-off between the high surface area with conductivity and stability, which remarkably determines the capacitor performance. In literature, the most practiced solution for the above problem is through compositing PANI with carbon morphologies, which includes graphene, carbon nanotubes (CNTs), carbon nano-

Received: January 18, 2015
Accepted: March 17, 2015
Published: March 18, 2015

DOI: 10.1021/acsami.5b00504
ACS Appl. Mater. Interfaces 2015, 7, 7661−7669

fibers (CNFs), etc.[17−20] Among these, graphene has added advantages of high surface area, better conductivity, and stability, along with its simple 2-dimensional (2-D) architecture.[21,22] However, the unavoidable restacking in the solution derived graphene results in considerably low surface area, which significantly hinders its prospect as a substrate to attain polymerization of aniline along its surface. This subsequently triggers polymerization outside the substrate, leading to the grains of bulk-phase polymer with all its inherent textural and property limitations. On the other hand, the spatially separated graphene sheets obtained through chemical vapor deposition (CVD) and other techniques are less viable due to the low yield and high cost involved in the production process.

One of the effective strategies adopted to avoid the restacking of graphene is by grafting organic molecules on its surface through covalent functionalization.[23,24] Steric hindrance between the anchored molecules helps the graphene layers to stay apart, which in turn improves the ionic accessibility while ensuring the other inherent properties intact. On the basis of this consideration, we have developed a simple and template-free strategy to construct a unique 3D PANI nanostructure impregnated through pillared graphene layers. The pillared graphene is synthesized by anchoring *p*-amino benzoic acid (PAB) molecules on the graphene surface through diazotization process.[25] The grafted benzoic acid (BA) molecule can act as a pillar to prevent the graphene from aggregation.[26] At the same time, the presence of the −COOH group in BA can be exploited as a nucleating as well as a binding site for aniline, which controls the rate of polymerization to achieve a compact and porous structure for G-PANI-PA. In situ preparation of 3D PANI has been achieved by a simple chemical oxidation of aniline in the presence of phytic acid (PA) and pillared graphene. Because of the chelating nature of PA, the 3D structure of polyaniline is formed (G-PANI-PA),[27] whereas lack of such a structure directing role by the conventional acids (HCl, H_2SO_4, etc.) leads to the formation of less porous PANI phase. The schematic representation of the synthetic procedure for G-PANI-PA is illustrated in Scheme 1.

Scheme 1. Schematic Representation of the Stages Involved in the Synthesis of Benzoic Acid (BA) Functionalized Graphene through Diazotization Reaction and Further Formation of the 3D Polyaniline Hybrid Structure (G-PANI-PA) As Mediated by Phytic Acid (PA) as a Dopant

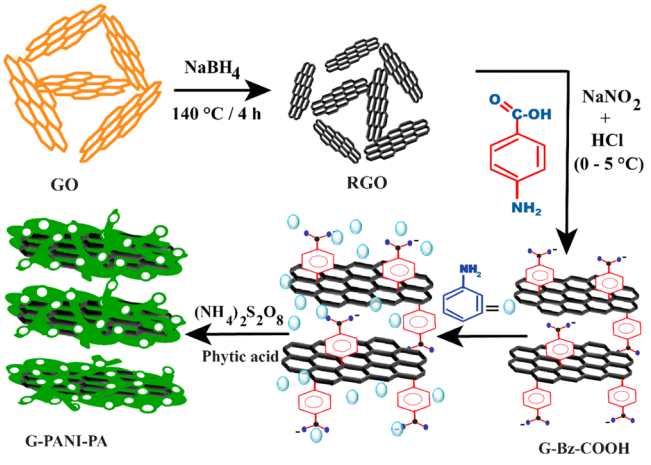

2. EXPERIMENTAL SECTION

Materials. Graphite powder, potassium permanganate ($KMnO_4$), *p*-amino benzoic acid (PAB), hydrogen peroxide (30%), aniline, ammoniumpersulfate $(NH_4)_2S_2O_8$, phytic acid, and *N*-methylpyrrolidone (NMP) were procured from M/s. Aldrich Chemicals. Sulfuric acid (H_2SO_4), ethanol, and hydrochloric acid (HCl) were procured from Rankem Chemicals. All the chemicals were used as received without any further purification. A polytetrafluoroethylene (PTFE) filter paper (pore size, 0.45 μm; Rankem) was used for the filtration. A copper grid with a carbon support (Ted Pella, Inc.) was used for the high-resolution transmission electron microscope (HRTEM) observations.

Synthesis of Pillared Graphene. The synthesis of pillared graphene was carried out as follows. Initially, the graphene oxide (GO) was prepared by modified Hummers method, as reported elsewhere.[28] Graphite and $KMnO_4$ (1:6 ratio) were mixed together, ground well, and slowly added in the acid mixture (H_2SO_4 and H_3PO_4) kept in an ice bath. Subsequently, the reaction mixture was transferred to an oil bath at 55 °C and the mixture was allowed to stir continuously for overnight. The resulting brown solid formed after the reaction was transferred to a beaker containing cold water with 3 mL of H_2O_2 (30%) to get a yellow solution. Subsequently, this was washed with HCl to remove metal impurities, followed by water, ethanol, and acetone, which gives the brownish GO solution. After drying at 60 °C, solid GO was obtained. Reduced graphene (RGO) was obtained by the reduction of GO with $NaBH_4$. In a typical reaction, GO (100 mg) was dispersed in water by sonication. Subsequently, 100 mL of aqueous solution of $NaBH_4$ (0.1 M) was added slowly with constant stirring in an ice bath. After the addition, the reaction mixture was allowed to stir in an oil bath, at 140 °C, for 4 h. Then, the mixture was allowed to cool at room temperature, followed by washing with water and ethanol, and finally dried at 60 °C. For making pillared graphene (G-Bz-COOH), a diazotization reaction was carried out. A known amount of RGO was dispersed in water by sonication. The diazonium solution (mixture of 100 mM $NaNO_2$ and *p*-amino benzoic acid (500 mM) in water) was added slowly to the RGO dispersion by maintaining the reaction temperature at 0−5 °C in an ice bath. Subsequently, concentrated HCl was added through the walls of the beaker to initiate the diazotization process. The reaction mixture was allowed to stir continuously for 12 h. The black color suspension was filtered, followed by washing with water and ethanol, and the wet cake was dried at 60 °C.

Synthesis of PANI-PA and G-PANI-PA Composites. Graphene polyaniline composite (G-PANI-PA) was prepared by in situ polymerization of aniline in the presence of phytic acid. Initially, aniline (1 M/0.74 mL) and G-Bz-COOH (100 mg) were dispersed in phytic acid (1 M/50 mL) and then the mixture was sonicated for 3 h to get a homogeneous dispersion. Followed by this, aqueous solution of ammonium persulfate 1.25 M (APS) was added slowly to the aniline-graphene mixture in an ice bath at 0−5 °C. The reaction was allowed to stir for overnight to get a green solid. The resulting material was filtered and dried at 60 °C to get the composite. The same procedure was followed, except the addition of graphene, to make the 3D-polyaniline (PANI-PA). To understand the role of the acid in altering the morphological characteristics of the PANI phase, two samples, designated as PANI-HCl and PANI-HS, were also obtained by following the aforementioned protocol and by replacing phytic acid with HCl and H_2SO_4, respectively. Finally, controlled experiments were done by using pristine graphene (without functionalization, i.e., RGO) by maintaining the monomer content as 60% and the corresponding sample is denoted as p-G-PANI-PA.

Electrode Making. The electrodes were prepared by coating a thin film of the PANI based samples (a paste was made by mixing the PANI samples with NMP) onto 1 cm^2 area of a Toray carbon paper. An excess dimension outside the sample coated area was kept to utilize it as the current collector during the measurements. The electrodes were dried overnight at 100 °C. The CV measurements were taken at different scan rates from 10 to 500 mV/s by maintaining a potential

DOI: 10.1021/acsami.5b00504
ACS Appl. Mater. Interfaces 2015, 7, 7661−7669

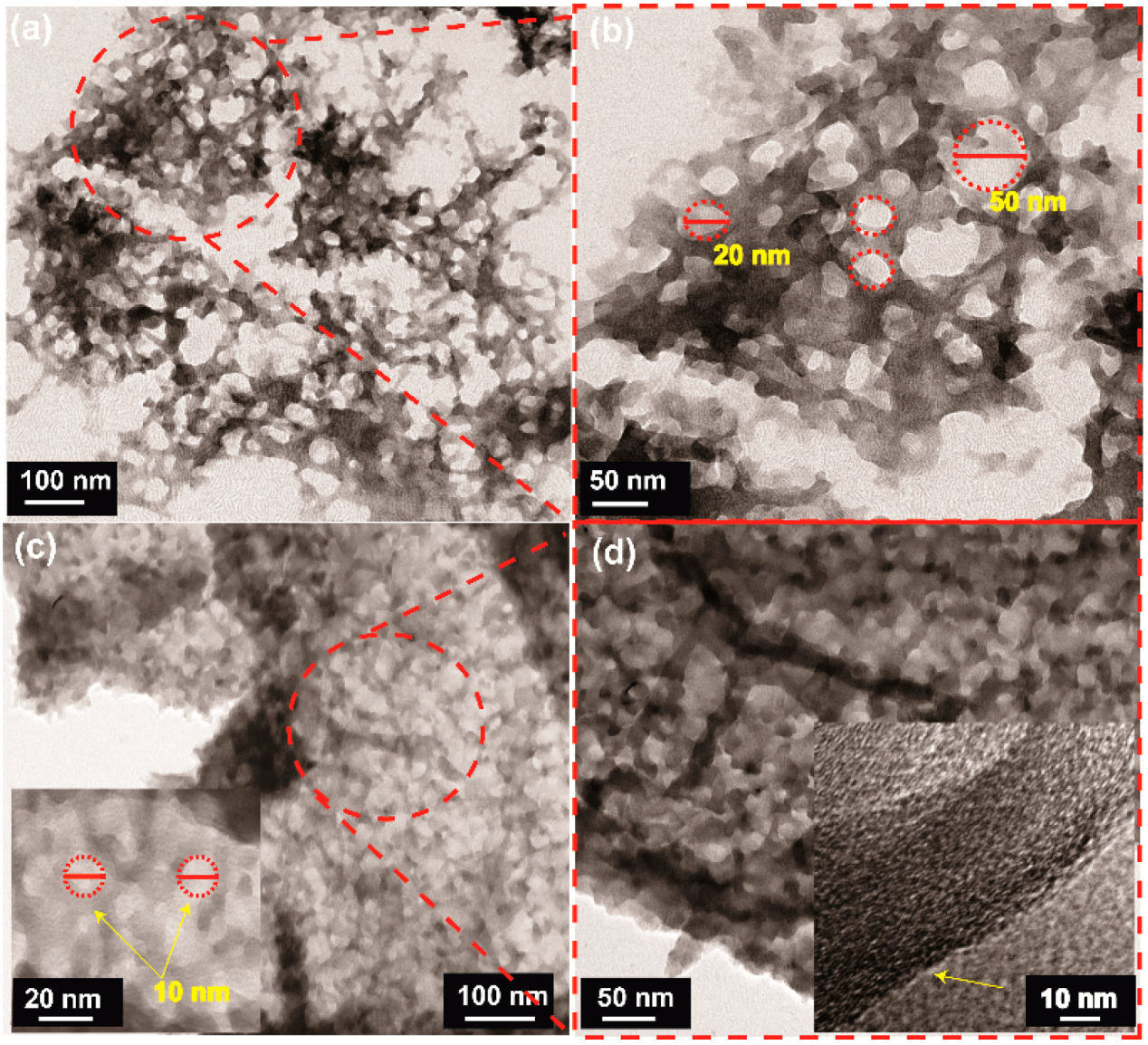

Figure 1. TEM images of (a) phytic acid mediated polyaniline (PANI-PA), (b) magnified image of the portion marked in (a), (c) PANI-graphene nanostructure (G-PANI-PA) indicating the porous and interpenetrated PANI layer on the graphene sheets, and (d) magnified view of the portion highlighted in (c); the inset shows the disordered graphitic lattice fringes.

window between 0 and 0.8 V in a symmetrical two-electrode configuration using 0.5 M H_2SO_4 as an electrolyte.

Fabrication of Solid-State Supercapacitor. A solid-state supercapacitor device was made by sandwiching PVA-H_2SO_4 gel electrolyte between two PANI coated carbon papers. After drying at 60 °C for 6 h, the cell was directly used for the supercapacitor performance. Four such single cells were connected in series to make a single device and lightened an LED having an operating potential of 1.5 V. The charge−discharge (CD) measurements were performed at a current density of 5 A/g by maintaining a potential window between 0 and 2.4 V (details are given in Supporting Information).

Characterization. The powder X-ray diffraction (PXRD) data of the materials were taken on a PANalytical X'pert Pro instrument with a scan rate of 0.5° per min, using Cu Kα (1.5418 Å) radiation. The structural and morphological information was obtained by using a high-resolution transmission electron microscope FEI model TECNAI G^2 F30 instrument, which was at an accelerating voltage of 300 kV (Cs = 0.6 mm, resolution 1.47 Å). Dilute suspensions of the samples were made by dispersing the prepared material in isopropyl alcohol. The samples required for the TEM analysis were prepared by drop-casting the suspension onto a 200-mesh copper grid coated with carbon film (Ted Pella, INC) and drying under a lamp overnight. A scanning electron microscope (SEM) system (FEI, model Quanta 200 3D) equipped with EDX (energy dispersive X-ray) analysis attachment at an operating potential of 30 kV was also used for obtaining further morphological information. Raman analysis of RGO and G-Bz-COOH was performed on an HR 800 Raman spectrometer (Jobin Yvon, Horiba, France) using 632 nm laser (NRS 1500 W) in order to obtain information on the graphitic and defective nature of the carbon. Nitrogen adsorption−desorption experiments were conducted at 77 K in a Quantachrome Quadrasorb automatic volumetric instrument using ultrapure N_2 (99.9%). For the gas adsorption measurements, the samples were preactivated at room temperature (for 24 h) and 100 °C (for 36 h) under ultrahigh vacuum (10−8 mbar) overnight. A PerkinElmer STA 6000 analyzer was used to perform thermogravimetric analysis by ramping the temperature from room temperature to 900 °C with a heating rate of 10 °C min^{-1} in air atmosphere. All the electrochemical experiments were done by using a *BioLogic* VMP3 instrument. Cyclic voltammetry (CV) analysis was carried out in a symmetrical two-electrode setup (potential range of 0−0.8 V) where PANI coated carbon paper was used as a working electrode. The chrono charge−discharge (CD) analysis was done at different current

DOI: 10.1021/acsami.5b00504
ACS Appl. Mater. Interfaces 2015, 7, 7661−7669

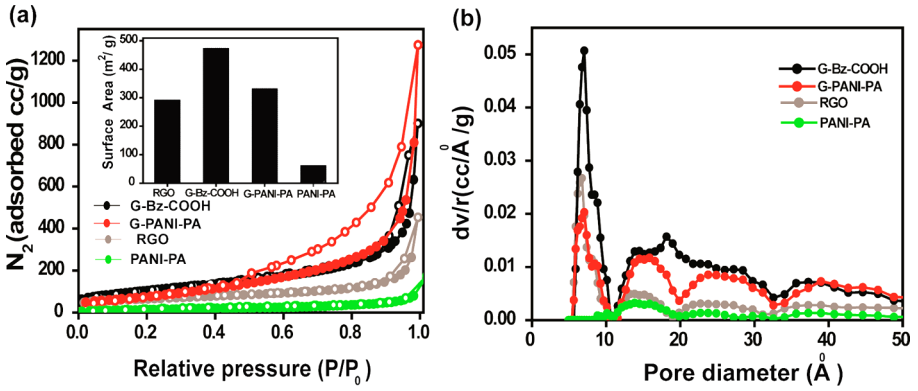

Figure 2. (a) BET surface area analysis of a PANI-PA, RGO, G-PANI-PA, and G-Bz-COOH with the inset bar graph showing the measured surface area for the corresponding samples and (b) comparative pore size distribution plots for the corresponding samples.

densities (0.5−20 A g^{-1}) in the same potential range that was used for CV. Cycling stability was done by chrono charge−discharge method at 5 A/g current density for 4000 continuous cycles. Electrochemical impedance (EIS) analysis was carried out from 1 MHz to 0.01 Hz frequency against the open circuit potential with a sinus amplitude of 10 mV (V_{rms} = 7.07 mV). The analysis of the EIS data was performed using an ECLab Software v10.19.

3. RESULTS AND DISCUSSION

The TEM images in Figure 1a and b clearly depict that the bulk PANI formed by using PA (PANI-PA) achieves an interconnected 3D network structure with evenly distributed mesopores. On the other hand, the HCl and H_2SO_4 derived PANI samples, i.e., PANI-HCl and PANI-HS, respectively, show highly dense nanofiber and platelike morphologies (Figures S1 and S3, Supporting Information). This alteration in the growth pattern of PANI formed from the different acids is expected to make a significant difference in the accessibility of the surface and, thereby, the interfacial chemistry and charge storage properties. The PANI morphology derived from PA is interesting in this context due to its well-defined 3D architecture and voids between the interconnected arms. Figure 1b indicates that the voids between the interconnected arms of PANI are in the range of 20−50 nm, which are clearly formed by the 3D interconnection of the polymer units. Formation of these types of 3D structured growth pattern of a conducting polymer like PANI, which simultaneously attains well-distributed pores and interconnected polymer matrix, is very important in an application like a supercapacitor, where the establishment of the electrode−electrolyte interfacial area and continuity in the conducting phase are the two key activity determining factors.

The field emission scanning electron microscope (FE-SEM) images in Figure S2a and b, Supporting Information, show the clear difference between the morphologies of RGO and G-Bz-COOH. RGO shows stacked graphene layers whereas G-Bz-COOH indicates wrinkled graphene layers with more macro- and mesopores. This morphological difference is expected to originate from the pillaring of Bz-COOH groups on graphene layers, and this is further well supported by the surface area analysis. Figure 1c corresponds to the pillared graphene−PANI-PA composite (G-PANI-PA), which clearly shows that the 3D polymer is distributed and aligned homogeneously on the graphene sheets. As discussed previously, the pillared graphene is formed by the benzoic acid functionalization of graphene (G-Bz-COOH). A close look at the morphologies of the PANI phases formed in G-PANI-PA and PANI-PA reveals good resemblance in the growth patterns of the PANI phases in both the cases. This indicates that the 3D PANI network could be effectively grafted on G-Bz-COOH when the reaction was carried out in the latter's presence. Such a uniform polymer wrapping was achieved through the formation of evenly distributed aniline moieties along the graphene planes through the interaction between the −COOH and $-NH_2$ groups present in G-Bz-COOH and aniline, respectively. The presence of the polymer layer between the graphene layers brings in contrast the difference between the PANI and graphene phases as evident in Figure 1c and d. The inset of Figure 1d shows the lattice fringes corresponding to the disordered graphene. The wavy nature of the lattice fringes depicts the intercalation of the PANI network through the pillared graphene layers. However, a reduction in the pore size from 20 to 50 nm to nearly 10 nm has been observed upon allowing PANI-PA to grow on the graphene surface. This is attributed mainly to the interaction between the functional groups in G-Bz-COOH and aniline molecules, which further minimizes the rate of polymerization, thereby resulting in reduction in the pore size.

An evidence for the porous structure of the pillared graphene has been obtained from the enhancement in the surface area of G-Bz-COOH (472 m ^{2}/g) in comparison with RGO (290 m^2/g) through BET (Brunauer−Emmett−Teller) measurements (Figure 2a and Table 1). The N_2 adsorption isotherm reveals

Table 1. Comparison of the Specific Capacitance (CV and CD Studies) and Electrical Conductivity (Four-Probe Method) Obtained for All the Prepared Samples

s. no.	sample	specific capacitance (F/g) (error limit ± 5)	electrical conductivity (S/cm) (error limit ± 0.05)	density (g/cm^3) (error limit ± 0.03)	surface area (m^2/g)
1	RGO	70	3.00	0.74	290
2	G-Bz-COOH	130	1.20	0.58	472
3	PANI-PA	512	2.70	0.64	60
4	G-PANI-PA	652	3.74	0.68	330
5	p-G-PANI-PA	415	2.10		220
5	PANI-HCl	435	4.20	0.72	34
6	PANI-HS	389	3.40		19

DOI: 10.1021/acsami.5b00504
ACS Appl. Mater. Interfaces 2015, 7, 7661−7669

the presence of a wide distribution of pores from micro to meso ranges (pore width of 1−3 nm), and the estimated pore volume for G-Bz-COOH is 1.072 cc/g, which is significantly higher than that of RGO (0.367 cc/g). The pore size distribution plot reveals a major micropore contribution in G-Bz-COOH compared to RGO (Figure 2b), and the pore size is also larger than the size of the electrolyte ions (0.5−0.75 nm).[29] This clearly suggests that functionalization is likely to improve the accessibility of the external molecules toward the graphene layers and facilitates faster ion movements in and out during charging and discharging. Along with this, the measured surface area for PANI-PA is 60 m^2/g, which is found to be larger than the surface areas obtained for the PANI samples prepared by using the acids like H_2SO_4 (PANI-HS, 19 m^2/g) and HCl (PANI-HCl, 34 m^2/g). The higher surface area of PANI-PA is credited to the 3D chelating feature of PA, which triggers formation of 3D and highly porous network of PANI (Figure S4, Supporting Information).

The four-probe based electrical conductivity measurement shows that the order of conductivity for PANI samples follows as PANI-HCl (4.20 S/cm) > PANI-HS (3.40 S/cm) > PANI-PA (2.70 S/cm). The high porosity of PANI-PA results in its low conductivity compared to the rest of the samples. However, upon the intercalated growth of PANI-PA on graphene (i.e., G-PANI-PA), the presence of the graphene layer underneath the PANI-PA phase results in short-circuiting the conducting path, leading to an improved conductivity of 3.74 S/cm. It should be noted that this improvement in conductivity is maintained concomitantly with a surface area of 330 m^2/g and a pore volume of 0.606 cc/g for G-PANI-PA. Moreover, the surface area (224 m^2/g) and electrical conductivity (1.52 S/cm) values were also measured for PANI-G-Bz-COOH physical mixture samples (details are given in Supporting Information), which are found to be significantly lower than the present system of interest (Figure S11, Supporting Information). Hence, it again proves the role of functional groups for effective anchoring of PANI to simultaneously tune both the surface area and the electrical conductivity. The density measurement shows that the order of density for the samples G-PANI-PA, PANI-PA, and G-Bz-COOH follows the order 0.74 (RGO) > 0.68 (G-PANI-PA) > 0.64 (PANI-PA) > 0.58 g/cm^3 (G-Bz-COOH) (Table 1). It clearly suggests that the minimum density accounted for G-Bz-COOH compared to RGO is mainly attributed to the formation of spatially separated graphene layers after functionalization. It is interesting to note that the increased surface area of G-PANI-PA (330 m^2/g) does not result in low density. The interaction between the functional groups present in G-Bz-COOH reduces the rate of polymerization, which leads to the attainment of a compact structure for G-PANI-PA. This is again well supported by the enhanced electrical conductivity (3.54 S/cm) and slight reduction in the surface area (330 m^2/g) for G-PANI-PA. In addition, the measured density for PANI-HCl (0.72 g/cm^3) is comparatively higher than that of PANI-PA (0.64 g/cm^3) due to the formation of bulk polymer phase using HCl compared to the 3D morphology conceived by PA.

The functionalization of BA on RGO (G-Bz-COOH) is unravelled using Fourier transform infrared (FT-IR) spectra analysis. The spectra of G-Bz-COOH (Figure 3), which displays an increased area under the sharp peak at 1705 cm^{-1} in comparison to RGO, validate the increased density of the −COOH groups. Further, a shift from 1705 to lower frequency 1690 cm^{-1} of the −C═O peak in G-PANI-PA attributes the

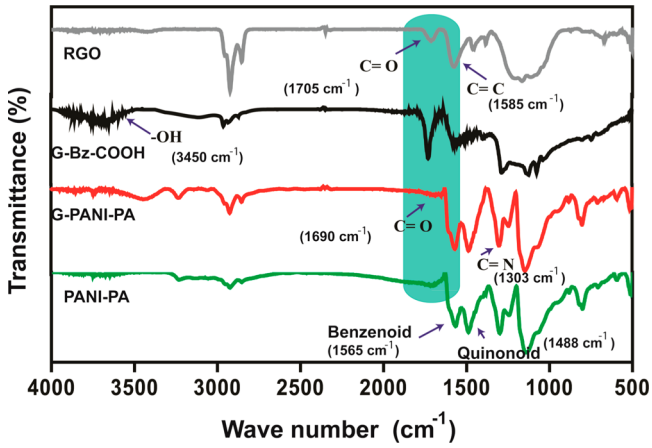

Figure 3. FT-IR spectra of RGO, G-Bz-COOH, G-PANI-P,A and PANI-PA.

strong interaction between the −COOH and $-NH_2$ groups of G-Bz-COOH and PANI. The Raman spectra of RGO and G-Bz-COOH exhibit bands at similar positions of 1333 and 1595 cm^{-1}, which correspond to the disordered graphitic diamond structure (D band) and crystalline graphitic carbon (G band), respectively. Grafting of BA molecules on graphene leads to more of the sp^3 type carbons, which has been proved again by the higher I_D/I_G ratio of G-Bz-COOH (1.46) compared to that of RGO (1.21) (Figure S5, Supporting Informtion). Figure S6, Supporting Information, gives the PXRD patterns of the prepared samples. The PXRD pattern of RGO shows two peaks centered at 2θ value of 25.5 and 44.0°, corresponding to the diffractions from the (002) and (100) graphitic carbon planes, respectively, and depicts the highly crystalline nature and efficient conversion of GO into graphene. In the case of G-PANI-PA, three main peaks positioned at 13, 20.6, and 25.1°, corresponding to the (011), (020), and (200) crystal planes of PANI, respectively, are present, which are observable in the bulk PANI as well. The thermogravimetric analysis (TGA) profile given in Figure S7, Supporting Information, reveals that the initial weight loss at 150 °C for G-PANI-PA is due to the elimination of the functional groups present in G-Bz-COOH. The weight loss observed in the second region at ∼250 °C is attributed to the oxidative degradation of the polymer, which is completely oxidized at ∼650 °C. Further quantification indicates that nearly 40 wt % of graphene is present in G-PANI-PA.

To understand the effect of improved surface area and conductivity of G-PANI-PA for charge storage applications, cyclic voltammetry (CV) and charge−discharge (CD) analysis were performed in a symmetrical two-electrode fashion, using 0.5 M H_2SO_4 as the electrolyte. Initially, we have tried to estimate the capacitance contributions by G-Bz-COOH and PANI-PA before going for a detailed investigation using G-PANI-PA. The CV profiles for G-Bz-COOH are rectangular in shape with an improved capacitance of 130 F/g and the sample display high capacitance retention value in comparison with 70 F/g recorded for RGO (Figure 4a and b). This enhancement in the capacitance of G-Bz-COOH is primarily credited to the surface area enhancement accomplished by the system by spatially separating the graphene layers through pillaring via the BA functionalities, which aids faster ion movement inside the layers. Moving to the CV profile of pure 3D PANI, i.e., PANI-PA, a fairly rectangular shape along with its well-known two

DOI: 10.1021/acsami.5b00504
ACS Appl. Mater. Interfaces 2015, 7, 7661−7669

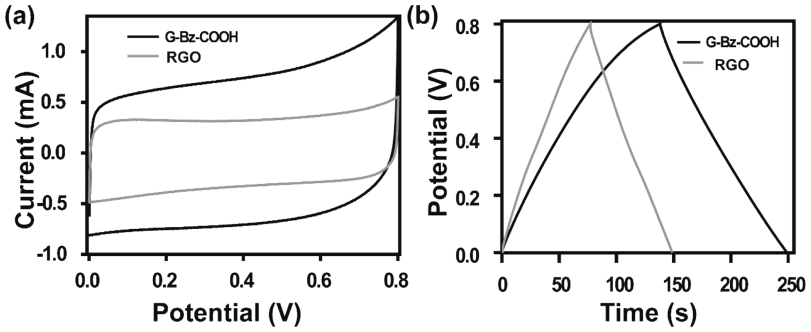

Figure 4. (a) Comparative cyclic voltammograms of RGO and G-Bz-COOH recorded at a scan rate of 10 mV/s in 0.5 M H_2SO_4 and (b) corresponding charge−discharge profiles measured at 1 A/g current density for RGO and G-Bz-COOH.

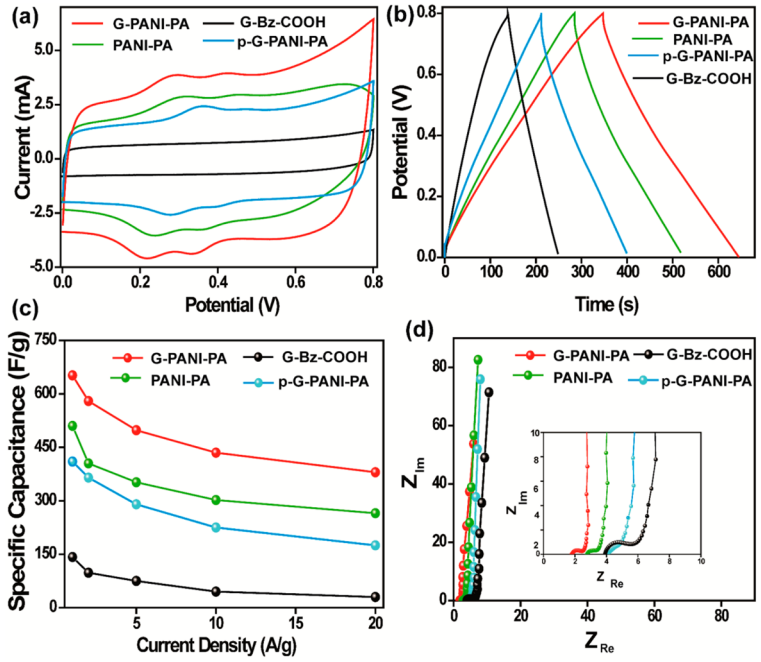

Figure 5. (a) Combined cyclic voltammograms taken at a scan rate of 10 mV/s in 0.5 M H_2SO_4, (b) charge−discharge profiles recorded at 1 A/g current density, (c) specific capacitance as a function of the current density for the samples, and (d) Nyquist plots of the prepared samples with the inset showing the enlarged part of the high-frequency region.

redox peaks corresponding to the transformation between the leucoemeraldine to emeraldine and the emeraldine to pernigraniline states are observed[30] (Figure 5a). In comparison with PANI-HCl and PANI-HS (Figure S8, Supporting Information), high double layer capacitive current has been observed in the case of PANI-PA. This results from the peculiar 3D architecture of the latter, which simultaneously achieves high surface area and porosity and, thereby, extended electrode−electrolyte interface. The calculated specific capacitance at a scan rate of 10 mV/s of PANI-PA is 512 F/g, which is substantially higher than those of PANI-HCl (435 F/g) and PANI-HS (389 F/g) (details are given in Supporting Information, Table S2). In addition, better ionic accessibility as expected from the 3D morphology of PANI-PA helps the system to display high capacitance retention (57%) at higher current drag conditions (10 A/g) where faster ionic mobility is required. Thus, the 3D morphology of PANI in PANI-PA is observed to be playing a vital role in modulating the electrode kinetics and enhancing the ionic conductivity, which altogether make the system a good supercapacitor electrode possessing high specific capacitance and capacitance retention (Figure 5c).

This unique morphology of PANI-PA could be implanted on the surfaces of the pillared graphene layers in G-PANI-PA, with an intention to further fine-tune the essential characteristics such as electrical conductivity and structural integrity. The layered graphene serves as a solid template that provides mechanical integrity and accessible channels for the electrolyte through the interlayer spacing. G-PANI-PA displays a specific capacitance of 652 F/g at 10 mV/s (Figure 5a). This corresponds to a mass specific capacitance of 875 F/g for PANI in the composite, by accounting for the capacitance contribution from G-Bz-COOH (details of the calculation are given in Supporting Information). This enhancement in capacitance clearly underlines the role played by the improved interface and ionic accessibility along with the high electrical conductivity of G-PANI-PA. To further validate the enhanced performance of the samples, charge−discharge analysis was performed and the corresponding data are presented in Figure 5b. It can be seen that G-PANI-PA shows ∼65% retention in capacitance compared to 57% displayed by PANI-PA (Figure 5c). The results are further substantiated by electrochemical impedance spectroscopic (EIS) analysis (Figure 5d and Figure

DOI: 10.1021/acsami.5b00504
ACS Appl. Mater. Interfaces 2015, 7, 7661−7669

S9, Supporting Information). The output is given in the form of a Nyquist plot, which shows the frequency response of the electrode/electrolyte system and is formed by plotting the imaginary component (Z″) of the impedance against the real component (Z′). The Nyquist plots of G-PANI-PA, PANI-PA, PANI-HCl, and PANI-HS exhibit a semicircle in the high-frequency range, followed by a straight sloped line in the low-frequency region. The diameter of the high-frequency semicircle corresponds to the charge transfer resistance (RCT) of the electrode kinetics. Among the samples, G-PANI-PA possesses a RCT of 0.67 Ω, which is significantly lower than that of the other samples (G-Bz-COOH, 1.2 Ω; PANI-PA, 0.79 Ω; PANI-HCl, 1.79 Ω; and PANI-HS, 1.84 Ω). Further, it proves the enhanced ionic mobility originated from the 3D architecture of the PANI morphology in PANI-PA. The large RCT accounted for G-Bz-COOH (1.2 Ω) might be due to the pillaring of the nonconducting organic molecules (Bz-COOH) on the graphene surface. Although G-Bz-COOH shows high RCT values, its enhanced surface area (472 m^2/g) helps to display an improved specific capacitance (130 F/g) compared to RGO (70 F/g).

To confirm the effect of the spatially separated graphene layers for bringing in the enhanced charge storage characteristics of G-PANI-PA, a comparison on the electrochemical activity is made by using a PANI composite derived from nonfunctionalized (pristine) graphene (p-G-PANI-PA). The measured capacitance for p-G-PANI-PA (415 F/g) is substantially lower than that of the present system of interest (Figure 5a, b, and c). Here, the lack of anchoring sites and tendency of restacking of the graphene layers decrease the amount of aniline moieties that can be anchored on the graphene surface (Figure S10, Supporting Information). Eventually, this leads to the formation of a good amount of PANI in the bulk phase with all the structural and morphological limitations to serve as a good charge storage material.

Controlled experiments were performed by tuning the aniline and G-Bz-COOH ratios. Compared to G-Bz-COOH, after incorporation of PANI in the case of G-PANI-PA-25, an increase in the specific capacitance to 310 F/g is observed. G-PANI-PA displays a maximum specific capacitance of 652 F/g with 60% PANI loading, which is comparatively higher than the capacitance measured from the other composites like G-PANI-PA-25 (310 F/g) and G-PANI-PA-75 (580 F/g). The increase in the PANI loading beyond a threshold level leads to a deviation from the rectangular behavior of the CV curves as evident in the case of G-PANI-PA-75 (Figure S12 a and b, Supporting Information). This is mainly attributed to the reduction in the surface area and the formation of bulk PANI phase during the higher loading and the associated change in the electrical conductivity (Table S1, Supporting Information).

The specific capacitance is found to be strongly influenced by the mass loading of the material on the electrode. This has been studied by varying the mass loading of G-PANI-PA as 0.5, 1.0, 2.0, and 3.0 mg/cm^2. The specific capacitance follows the order 1084 > 652 > 580 > 510 F/g for the loading of 0.5, 1.0, 2.0, and 3.0 mg/cm^2, respectively. It should be noted that, even with a mass loading as high as 3 mg/cm^2, the system succeeds in displaying a specific capacitance of 510 F/g, which helps to provide an areal capacitance of 1.02 F/cm^2 and a volumetric capacitance of 122 F/cm^3 (details are given in Figure 6a and b and in Tables S2 and S3, Supporting Information). The present work is also compared with the recently reported 3D PANI/carbon based electrode materials. Wei et al. reported a hierarchical porous graphene/polyaniline composite based supercapacitor with a specific capacitance of 385 F/g.[15] The present system highlights a specific capacitance of 652 F/g with excellent cycle stability (>90% retention) after 4000 cycles. These values are comparatively higher than that reported recently on the PANI based electrode materials (Table 2).

Table 2. Comparative Performance of the Present System of Interest with a Loading of 1.0 mg/cm^2 (Active Material) and a Current Density of 2 A/g, with the Literature Reported Systems

materials	specific capacitance (F/g)	electrolyte	conductivity (S/cm)	reference
in this work	652	H_2SO_4 (0.5 M)	3.74	
GO, PANI, $CaCO_3$	385	H_2SO_4 (1 M)		15
GO/PANI	250	H_2SO_4 (1 M)	8.66	30
PANI/MnO_2 template	477[a]	H_2SO_4 (1 M)		12
PANI/polymeric stabilizer, poly(*N*-vinylpyrrolidone)	55	H_2SO_4 (1 M)		13
PANI/GO	480	H_2SO_4 (2 M)	1.43	27
PANI/graphene nanoribbon	340[b]	H_2SO_4 (1 M)		21
PANI/CNF	638	H_2SO_4 (1 M)		20
flexible graphene/polyaniline	763	H_2SO_4 (1 M)		31
polyaniline/reduced GO	431	H_2SO_4 (1 M)	**906**	32

[a]Specific capacitance calculated for H_2SO_4 as an electrolyte. [b]Specific capacitance compared with a current density of 2 A/g.

To clearly make a judgment on the stability aspects of the materials, the charge−discharge analysis for PANI-PA and G-PANI-PA was performed up to 4000 cycles at a current density of 5 A/g under identical conditions. This leads to a 40% reduction in the capacitance in the case of PANI-PA (Figure 6b), which might be due to the shrinking and swelling of the polymer phase during the cycling process. G-PANI-PA, on the other hand, after a slight initial drop, displays a steady improvement in the capacitance up to 4000 cycles. This ensures almost 100% columbic efficiency by the system. This is mainly attributed to the establishment of better contact between the active material and the electrolyte over the cycling period. In other words, the porous skeleton of the active material improves the electrolyte penetration, which enhances the cycle life and thus validates the improved performance of G-PANI-PA.

Finally, to validate the application of the system in a realistic perspective, we fabricated a solid-state supercapacitor device by connecting four cells in series. A single cell and four cells in series show a specific capacitance of ∼512 and 387 F/g (at a current density of 1 A/g), respectively, which is comparable to the single cell having an area of 1 cm^2 (652 F/g) in 0.5 M H_2SO_4 (liquid electrolyte). The device thus obtained was used for illuminating an LED that has a working potential of 1.5 V, which shows the practical demonstration (Figure 6c). The LED glowed continuously brighter for 2 min, and thereafter the

DOI: 10.1021/acsami.5b00504
ACS Appl. Mater. Interfaces 2015, 7, 7661−7669

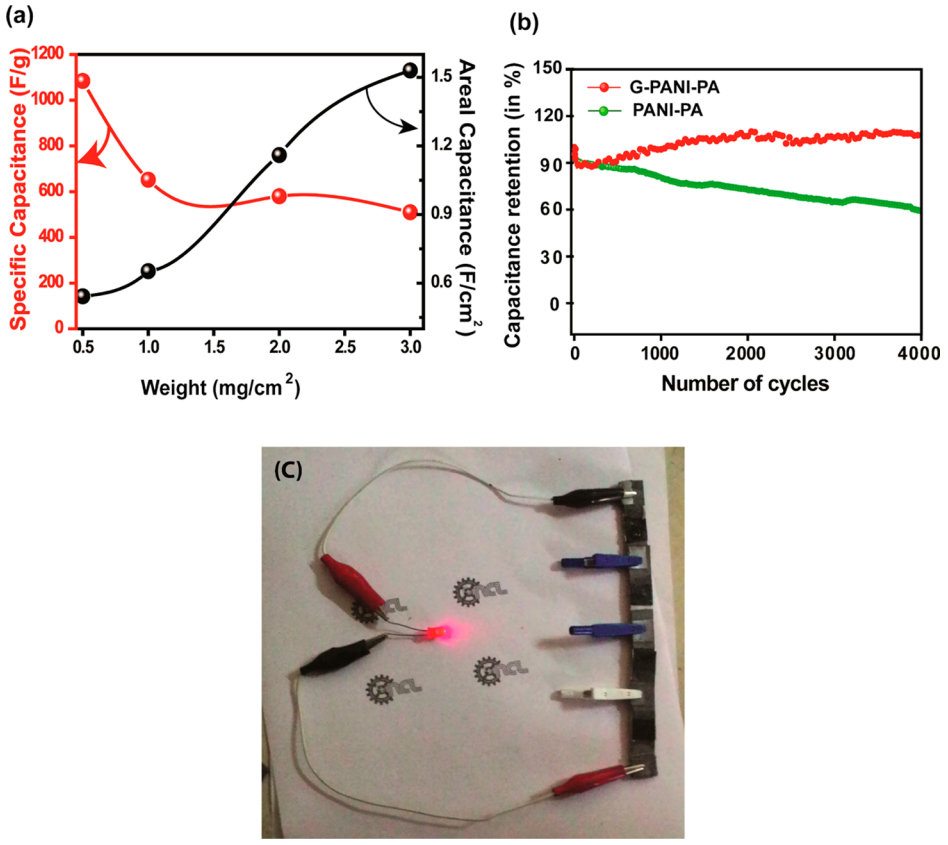

Figure 6. (a) Calculated specific capacitance and areal capacitance corresponding to the different loading of G-PANI-PA, (b) cycle stability behavior of G-PANI-PA and PANI-PA measured at a dragging condition of 5 A/g current density, and (c) the homemade solid-state supercapacitor device (four cells connected in series) used to illuminate an LED.

brightness reduced when the potential reached 2 V and the lighting lasted even after 5 min (details are given in Supporting Information and Figure S13).

4. CONCLUSION

In conclusion, a combination of diazotization reaction and in situ polymerization technique has been employed to construct a highly porous PANI graphene nanostructure (G-PANI-PA) that possesses a 3D structured PANI growth pattern aligned on chemically pillared graphene layers. The engineered material shows a high mass specific capacitance of 875 F/g with 65% retention ability even at a high current density of 10 A/g. Furthermore, the G-PANI-PA based supercapacitor shows better stability, so that even after 4000 cycles the system could maintain superior capacitance retention and almost 100% columbic efficiency. The strategy gives a feasible way to concomitantly address the prevailing issues of polyaniline such as its low surface area, sluggish ionic accessibility, and polymer degradation. A demonstration of a working supercapacitor model that was used to light an LED substantiates the experimental proofs on the promising electrochemical charge storage properties of the hybrid material.

■ ASSOCIATED CONTENT

Supporting Information

TEM, SEM analysis of the prepared samples, Raman analysis of RGO and G-Bz-COOH samples, IR study, BET surface area plots, TGA study of the prepared samples, electrical conductivity measurements and calculations (four-probe method), detailed specific capacitance calculations, surface area estimation for physical mixture composite, CV analysis of the PANI-HCl, HS samples, electrochemical impedance study, and additional supporting data. This material is available free of charge via the Internet at http://pubs.acs.org/.

■ AUTHOR INFORMATION

Corresponding Author

*E-mail: k.sreekumar@ncl.res.in. Tel.: +912025902566.

Notes

The authors declare no competing financial interest.

■ ACKNOWLEDGMENTS

The authors thank Dr. Sourav Pal, Director, CSIR-National Chemical Laboratory, Pune, for his constant support and for providing infrastructure. S.K. and P.S. acknowledge DST, India, for the financial support through the project no. SR/S1/PC05/2011.

■ REFERENCES

(1) Zhu, Y. W.; Murali, S.; Stoller, M. D.; Ganesh, K. J.; Cai, W.; Ferreira, P. J.; Pirkle, A.; Wallace, R. M.; Cychosz, K. A.; Thommes, M.; Su, D.; Stach, E. A.; Ruoff, R. S. Carbon-Based Supercapacitors Produced by Activation of Graphene. *Science* **2011**, *332*, 1537−1541.

(2) Wang, Y.; Xia, Y. Recent Progress in Supercapacitors: From Materials Design to System Construction. *Adv. Mater.* **2013**, *25*, 5336−5342.

(3) Dong, X.; Xu, H.; Wang, X.; Huang, Y.; Chan-Park, M.; Zhang, H.; Wang, L.; Huang, W.; Chen, P. 3D Graphene−Cobalt Oxide Electrode for High-Performance Supercapacitor and Enzymeless Glucose Detection. *ACS Nano* **2012**, *6*, 3206−3213.

DOI: 10.1021/acsami.5b00504
ACS Appl. Mater. Interfaces 2015, 7, 7661−7669

(4) Pech, D.; Brunet, M.; Durou, H.; Huang, P.; Mochalin, V.; Gogotsi, Y.; Taberna, P.; Simon, P. Ultrahigh-Power Micrometre-sized Supercapacitors Based on Onion-like Carbon. *Nat. Nanotechnol.* **2010**, *5*, 651−654.
(5) Madec, L.; Bouvr, A.; Blanchard, P.; Cougnon, C.; Brousse, T.; Lestriez, B.; Guyomarda, D.; Gaubicher, J. *In situ* Redox Functionalization of Composite Electrodes for High Power−High Energy Electrochemical Storage Systems *via* a Non-covalent Approach. *Energy Environ. Sci.* **2012**, *5*, 5379−5386.
(6) Lin, J.; Zhang, C. G.; Yan, Z.; Zhu, Y.; Peng, Z. W.; Hauge, R. H.; Natelson, D.; Tour, J. M. 3-Dimensional Graphene Carbon Nanotube Carpet-Based Microsupercapacitors with High Electrochemical Performance. *Nano Lett.* **2013**, *13*, 72−78.
(7) Zhou, C.; Zhang, Y.; Li, Y.; Liu, J. Construction of High-Capacitance 3D CoO @ Polypyrrole Nanowire Array Electrode for Aqueous Asymmetric Supercapacitor. *Nano Lett.* **2012**, *13*, 2078−2085.
(8) Simon, P.; Gogotsi, Y. Materials for Electrochemical Capacitors. *Nat. Mater.* **2008**, *7*, 845−853.
(9) Anothumakkool, B.; Kurungot, S. Electrochemically Grown Nanoporous MnO_2 Nanowall Forest on Porous Carbon Substrate with Enhanced Capacitance Through Faster Ionic and Electrical Mobility. *Chem. Commun.* **2014**, *50*, 7188−7190.
(10) Kumar, A.; Baek, J. B. Electrochemical Supercapacitors from Conducting Polyaniline-Graphene Platforms. *Chem. Commun.* **2014**, *50*, 6298−6308.
(11) Anothumakkool, B.; Torris, A. A. T.; Bhange, S. N.; Unni, S. M.; Badiger, M. V.; Kurungot, S. Design of a High Performance Thin All-Solid-State Supercapacitor Mimicking the Active Interface of Its Liquid-State Counterpart. *ACS Appl. Mater. Interfaces* **2013**, *5*, 13397−13404.
(12) Chen, W.; Rakhi, R. B.; Alshareef, H. N. Morphology-Dependent Enhancement of the Pseudocapacitance of Template-Guided Tunable Polyaniline Nanostructures. *J. Phys. Chem. C* **2013**, *117*, 15009−15019.
(13) Park, W.; Kim, T.; Huh, J.; Kang, M.; Lee, J. E.; Yoon, H. Anisotropic Growth Control of Polyaniline Nanostructures and Their Morphology-Dependent Electrochemical Characteristics. *ACS Nano* **2012**, *6*, 7624−7633.
(14) Kuila, B. K.; Nandan, B.; Bhome, M.; Janke, A.; Stamm, M. Vertically Oriented Arrays of Polyaniline Nanorods and their Super Electrochemical Properties. *Chem. Commun.* **2009**, *48*, 5749−5751.
(15) Meng, Y.; Wang, K.; Zhang, Y.; Wei, Z. Hierarchical Porous Graphene/Polyaniline Composite Film with Superior Rate Performance for Flexible Supercapacitors. *Adv. Mater.* **2013**, *25*, 6985−6990.
(16) Chmiola, J.; Largeot, C.; Taberna, P.; Simon, P.; Gogotsi, Y. Monolithic Carbide-Derived Carbon Films for Micro-Supercapacitors. *Science* **2010**, *328*, 480−483.
(17) Zhang, K.; Zhang, L. L.; Zhao, X. S.; Wu, J. Graphene/Polyaniline Nanofiber Composites as Supercapacitor Electrodes. *Chem. Mater.* **2010**, *22*, 1392−1401.
(18) Meng, C.; Liu, C.; Chen, L.; Hu, C.; Fan, S. Highly Flexible and All-Solid-State Paper like Polymer Supercapacitors. *Nano Lett.* **2010**, *10*, 4025−4031.
(19) Li, J.; Xie, H.; Li, Y.; Liu, J.; Li, Z. Electrochemical Properties of Graphene Nanosheets/Polyaniline Nanofibers Composites as Electrode for Supercapacitors. *J. Power Sources* **2011**, *196*, 10775−10781.
(20) Yan, X.; Tai, Z.; Chena, J.; Xue, Q. Fabrication of Carbon Nanofiber−Polyaniline Composite Flexible Paper for Supercapacitor. *Nanoscale* **2011**, *3*, 212−216.
(21) Li, L.; Raji, A. R. O.; Fei, H.; Yang, Y.; E. Samuel, L. G.; Tour, J. M. Nanocomposite of Polyaniline Nanorods Grown on Graphene Nanoribbons for Highly Capacitive Pseudocapacitors. *ACS Appl. Mater. Interfaces* **2013**, *5*, 6622−6627.
(22) Liu, F.; Song, S.; Xue, D.; Zhang, H. Folded Structured Graphene Paper for High Performance Electrode Materials. *Adv. Mater.* **2012**, *24*, 1089−1094.
(23) Huang, P.; Jing, L.; Zhu, H.; Gao, X. Diazonium Functionalized Graphene: Microstructure, Electric, and Magnetic Properties. *Acc. Chem. Res.* **2013**, *46*, 43−52.
(24) Zhang, H.; Li, Z.; Snyder, A.; Xie, J.; Stanciu, L. A. Functionalized Graphene Oxide for the Fabrication of Paraoxon Biosensors. *Anal. Chim. Acta* **2014**, *827*, 86−94.
(25) Li, Z.; Zhang, H.; Liu, Q.; Liu, Y.; Stanciu, L.; Xie, J. Covalently-Grafted Polyaniline on Graphene Oxide Sheets for High Performance Electrochemical Supercapacitors. *Carbon* **2014**, *71*, 257−267.
(26) Kumar, R.; Suresh, V. M.; Maji, T. K.; Rao, C. N. R. Porous Graphene Frameworks Pillared by Organic Linkers with Tunable Surface Area and Gas Storage Properties. *Chem.Commun.* **2014**, *50*, 2015−2017.
(27) Pana, L.; Yu, G.; Zhai, D.; Lee, H. R.; Zhao, W.; Liu, N.; Wang, H.; Tee, B. C. K.; Shi, Y.; Cuid, Y.; Bao, Z. Hierarchical Nanostructured Conducting Polymer Hydrogel with High Electrochemical Activity. *Proc. Natl. Acad. Sci. U.S.A.* **2012**, *109*, 9287−9292.
(28) Marcano, D. C.; Kosynkin, D. V.; Berlin, J. M.; Sinitskii, A.; Sun, Z.; Slesarev, A.; Alemany, L. B.; Lu, W.; Tour, J. M. Improved Synthesis of Graphene Oxide. *ACS Nano* **2010**, *4*, 4806−4814.
(29) Jiang, D.; Jin, Z.; Henderson, D.; Wu, J. Solvent Effect on the Pore-Size Dependent of an Organic Electrolyte Supercapacitor. *J. Phys. Chem. Lett.* **2012**, *3*, 1727−1731.
(30) Kumar, N. A.; Choi, H. J.; Shin, Y. R.; Chang, D. W.; Dai, L.; Baek, J. B. Polyaniline-Grafted Reduced Graphene Oxide for Efficient Electrochemical Supercapacitors. *ACS Nano* **2012**, *6*, 1715−1723.
(31) Cong, H. P.; Rena, X. C.; Wanga, P.; Yu, S. H. Flexible Graphene/Polyaniline Composite Paper for High Performance Supercapacitor. *Energy Environ. Sci.* **2013**, *6*, 1185−1191.
(32) Kim, M.; Lee, C.; Jyongsik, J. Fabrication of Highly Flexible, Scalable, and High-Performance Supercapacitors Using Polyaniline/Reduced Graphene Oxide Film with Enhanced Electrical Conductivity and Crystallinity. *Adv. Funct. Mater.* **2014**, *24*, 2489−2499.

DOI: 10.1021/acsami.5b00504
ACS Appl. Mater. Interfaces 2015, 7, 7661−7669